nature nanotechnology

LETTERS

PUBLISHED ONLINE: 30 JANUARY 2017 | DOI: 10.1038/NNANO.2016.300

Water-evaporation-induced electricity with nanostructured carbon materials

Guobin Xue[1†], Ying Xu[2†], Tianpeng Ding[1†], Jia Li[1†], Jun Yin[2], Wenwen Fei[2], Yuanzhi Cao[1], Jin Yu[2], Longyan Yuan[1], Li Gong[3], Jian Chen[3], Shaozhi Deng[3], Jun Zhou[1]* and Wanlin Guo[2]*

Water evaporation is a ubiquitous natural process[1] that harvests thermal energy from the ambient environment. It has previously been utilized in a number of applications[2,3] including the synthesis of nanostructures[4] and the creation of energy-harvesting devices[5,6]. Here, we show that water evaporation from the surface of a variety of nanostructured carbon materials can be used to generate electricity. We find that evaporation from centimetre-sized carbon black sheets can reliably generate sustained voltages of up to 1 V under ambient conditions. The interaction between the water molecules and the carbon layers and moreover evaporation-induced water flow within the porous carbon sheets are thought to be key to the voltage generation. This approach to electricity generation is related to the traditional streaming potential[7], which relies on driving ionic solutions through narrow gaps, and the recently reported method of moving ionic solutions across graphene surfaces[8,9], but as it exploits the natural process of evaporation and uses cheap carbon black it could offer advantages in the development of practical devices.

The experimental set-up for measuring water-evaporation-induced electric potential in a carbon black (CB) sample is illustrated in Fig. 1a. First, two electrodes made of multiwalled carbon nanotube (MWCNT) films were patterned on a quartz substrate (Supplementary Fig. 1 and Supplementary Movie 1). Then, a uniform CB sheet was collected on the substrate surface across the two electrodes over an ethanol flame[10], which was annealed at 370 °C for 2.5 h and treated by plasma for 1 min at a power of 130 W. Scanning electron microscopy characterization shows that the obtained CB sheet with thickness of about 70 μm consists of loosely aggregated nanoparticles with average diameter of ~20 nm (Supplementary Fig. 1), forming a specific surface area of ~167 $m^2 g^{-1}$ (Supplementary Fig. 2). High-resolution transmission electron microscopy (HR-TEM) indicates that each of the onion-like nanoparticles is basically formed of loosely stacked disordered graphene flakes (Fig. 1b). This is also confirmed by Raman spectroscopy[11,12] (Supplementary Fig. 3). After the annealing and plasma treatment, abundant functional groups are introduced to the CB samples as characterized by X-ray photoelectron spectroscopy (Supplementary Fig. 4) and the CB samples become hydrophilic so that water capillary action can occur along the samples.

The device, consisting of a CB sheet of size 1.0×2.5 cm^2 and two MWCNT electrodes with width of 2 mm, shows a robust ohmic contact between the CB sheet and electrodes (Supplementary Fig. 5). The copper wires connecting the electrodes were carefully covered by epoxy to avoid exposing them to water. After being fully infiltrated by deionized (DI) water (conductivity of $\sim 1.6 \times 10^{-4}$ S m^{-1}), the device was inserted into a 100 ml beaker with DI water covering the bottom end of the CB as illustrated in Fig. 1a. Surprisingly, an open-circuit voltage (V_{oc}) between the two electrodes is generated and gradually rises up to 1 V when the capillary water reaches its maximum height along the CB sheet in about 1 h (Fig. 1d, left inset). In all tests, the angle of the CB sheet with the water surface is about 57.3° in the beaker, and the capillary water can reach a height of about 2.0 cm. The induced voltage can reliably be maintained around 1 V during the whole test that lasts for 8 days with a stable short-circuit current (I_{sc}) around 150 nA (Supplementary Fig. 6) in the laboratory environment with the temperature fluctuating between 21.7 and 23.6 °C and relative humidity (RH) between 53.5 and 66%, as shown in Fig. 1d. The fluctuations in the measured voltage can be explained by the fluctuating laboratory temperature and humidity during the test.

When a capillary-saturated CB device with stable voltage around 0.85 V was sealed within the beaker, water evaporation from the CB surface gradually halted, and the induced voltage dropped accordingly and finally died out within 1,000 s; when we unsealed the system, the induced voltage rapidly returned to 0.85 V again. Such sealing- and unsealing-induced voltage change can be completely repeated as shown in Fig. 2a, indicating a strong correlation between the induced voltage and water evaporation. As water evaporates faster in the wind, the wind can be used to enhance the induced voltage. (Supplementary Fig. 7). The enhancement increases with increasing wind speed and disappears when the wind stops (Fig. 2b). Wind at speed of 2.9 m s^{-1} can raise the voltage from ~0.8 to ~1.5 V. The induced voltage can also be significantly suppressed from 1.1 to 0.25 V by increasing the humidity from 45 to 90% at a fixed temperature of ~22 °C (Fig. 2c and Supplementary Fig. 8). In our experiment, when the environmental temperature rises from 21.4 to 25 °C, the relative humidity drops accordingly from 75 to 60% and the induced voltage rises significantly from ~0.8 to ~1.8 V, as shown in Fig. 2d. As a decrease in humidity from 75 to 60% at a fixed temperature can only raise the induced voltage by about 0.5 V, as read from Fig. 2c, the remaining 0.5 V increment should be attributed to the 3.6 °C increase in temperature.

To further confirm the evaporation as the origin of the induced voltage, a seven-electrode device was used. As shown in the inset in Fig. 2e, the two bottom electrodes of a seven-electrode device are inserted into water while the rest of the electrodes are kept above the bulk water level, and the saturated voltages measured between each two neighbour electrodes, V_{1-2}, V_{2-3}, V_{3-4}, V_{4-5}, V_{5-6} and

[1]Wuhan National Laboratory for Optoelectronics, Huazhong University of Science and Technology, Wuhan 430074, China. [2]Key Laboratory for Intelligent Nano Materials and Devices of Ministry of Education, State Key Laboratory of Mechanics and Control of Mechanical Structures, Nanjing University of Aeronautics and Astronautics, Nanjing 210016, China. [3]State Key Laboratory of Optoelectronic Materials and Technologies, Guangdong Province Key Laboratory of Display Material and Technology, Sun Yat-sen University, Guangzhou 510275, China. †These authors contributed equally to this work.
*e-mail: jun.zhou@mail.hust.edu.cn; wlguo@nuaa.edu.cn

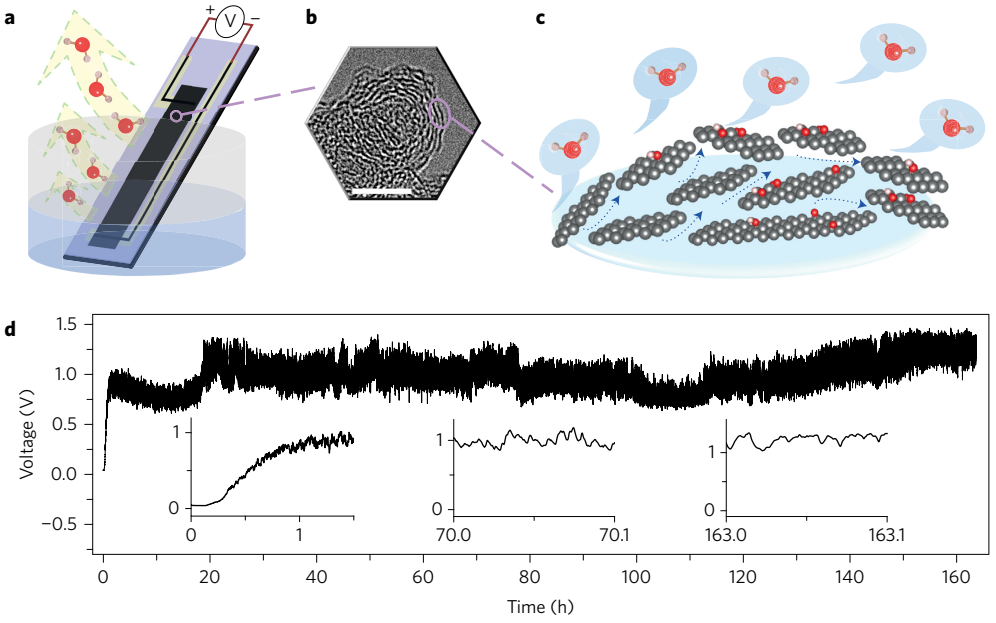

Figure 1 | Evaporation-induced electricity in CB. a, Schematic of device and experimental set-up for measuring evaporation-induced voltage. The device consists of a 1.0 × 2.5 cm^2 CB sheet and two 2-mm-wide MWCNT electrodes on a quartz substrate. The device was inserted into DI water for voltage measurements. **b**, Typical HR-TEM image of CB (purple circle in **a**). Scale bar, 5 nm. **c**, Schematic of the water evaporating from and induced water flow in CB (purple oval in **b**). **d**, Open-circuit voltage (V_{oc}) generated by water evaporation from the CB is sustained for 163 h under ambient laboratory conditions with fluctuations in relative humidity between 53.5 and 66% and room temperature between 21.7 °C and 23.6 °C during the test. The measured curves between 0 and 1.5 h, 70.0 and 70.1 h and 163.0 and 163.1 h are enlarged in the insets.

V_{6-7}, as well as between the two end electrodes 1 and 7, V_{1-7}, are presented in Fig. 2e. The measurement between each pair of electrodes lasts for about 80 s. As the two bottom electrodes 1 and 2 are immersed in the water, there is no measurable voltage V_{1-2}, indicating that no voltage can be generated in the immersed CB section without evaporation. The voltage between the two highest electrodes V_{6-7} is also zero, simply because capillary water cannot go beyond the sixth electrode. However, the rest of the CB sections show increasing voltages from V_{2-3} to V_{3-4}, to V_{4-5} and to V_{5-6}, because as the capillary height increases, the faster the water evaporates[13,14]. Even though there is no voltage in sections 1–2 and 6–7, which play the role of a conductor, a summation of V_{2-3}, V_{3-4}, V_{4-5} and V_{5-6} is equal to the measured V_{1-7}. Similar experimental results on more devices with multiple electrodes are presented in Supplementary Fig. 9. Once the CB sheet is further immersed by increasing the water level, the voltage will disappear in the newly immersed section and shift with a drop in the rest of the sections (Supplementary Fig. 10). When the whole device is immersed in water, the voltage signal becomes very weak (Supplementary Fig. 11). Careful investigation shows that the possible thermoelectric potential caused by the local temperature reduction during the water evaporation is four orders of magnitude weaker than the measured voltage (Supplementary Fig. 12). When the two-electrode device is turned over and the other end is dipped into the bulk water, the induced voltage reverses its sign but can reach the same amplitude (Fig. 2f).

All the results in Fig. 2 confirm that the sustainable voltage is indeed induced by water evaporation from the CB sheet. The possible mechanisms for the electricity generation should be the interactions of water molecules with the carbon materials, especially evaporation-induced water flow inside the porous carbon film. As the CB nanoparticles mainly consist of loosely stacked disordered graphene flakes, we calculated the charge redistribution caused by adsorption of water molecules on graphene flakes with different functional groups by density functional theory[15–17]. When a graphene flake with a C–O–C group is covered by three layers of water, a specific electric double layer forms at the water/graphene interface with an electron depletion of about 0.7*e* in the graphene layer (Fig. 3a). In comparison, the electron depletion drops to 0.0003*e* when the C–O–C group is removed (Fig. 3b). To understand the effect of functional groups for the electricity generation, further detailed experimental evidences are obtained. First, Fourier transform infrared spectroscopy (FTIR) shows significantly enhanced vibration peaks of O–H, C–O and C=O bonds[18] (Fig. 3c). X-ray photoelectron spectroscopy (XPS) characterizations further confirm the existence of these functional groups as well as C–OH, C–O–C, C=O and O=C–OH groups (Supplementary Fig. 5). As a result, the treatment turns the CB sheet from hydrophobic to hydrophilic, with the contact angle dropping from 143.25° to 10.15° (insets of Fig. 3c and Supplementary Fig. 13). As shown in Fig. 1d, the saturated V_{oc} in the treated CB sheet is about 1 V; but for the pristine hydrophobic CB device before treatment, water cannot go up along the CB film and the measured voltage can only rise to 45 μV, as detailed in Supplementary Fig. 14. This means that the annealing-and-plasma-treatment-induced functional groups are essential for the electricity generation in our system.

As sustaining evaporation of water from the surface of the CB film will certainly induce water flow up along the porous CB sheet (Fig. 1c), the streaming potential[7,19], an important classical electrokinetic effect created by driving ionic solutions through insulated narrow channels or porous media under a pressure gradient, should contribute to the measured voltage. To reveal the contribution of possible water-flow-induced potential driven by evaporation in the CB sheet, we designed a specific experiment as schematically shown in Fig. 3d. The bottom half of the CB sheet with two electrodes with a spacing of 5 mm is sealed in the beaker by a polyethylene (PE) membrane, while the top half of the CB sheet is exposed to ambient air. Evaporation of water from the CB section outside the PE membrane drives water flow along the porous CB sheet. This water flow can induce a voltage between the electrodes, as recorded in Fig. 3e, which is about 0.16 V without wind and can be enhanced to 0.27 V by wind outside the sealed beaker. As the humidity inside

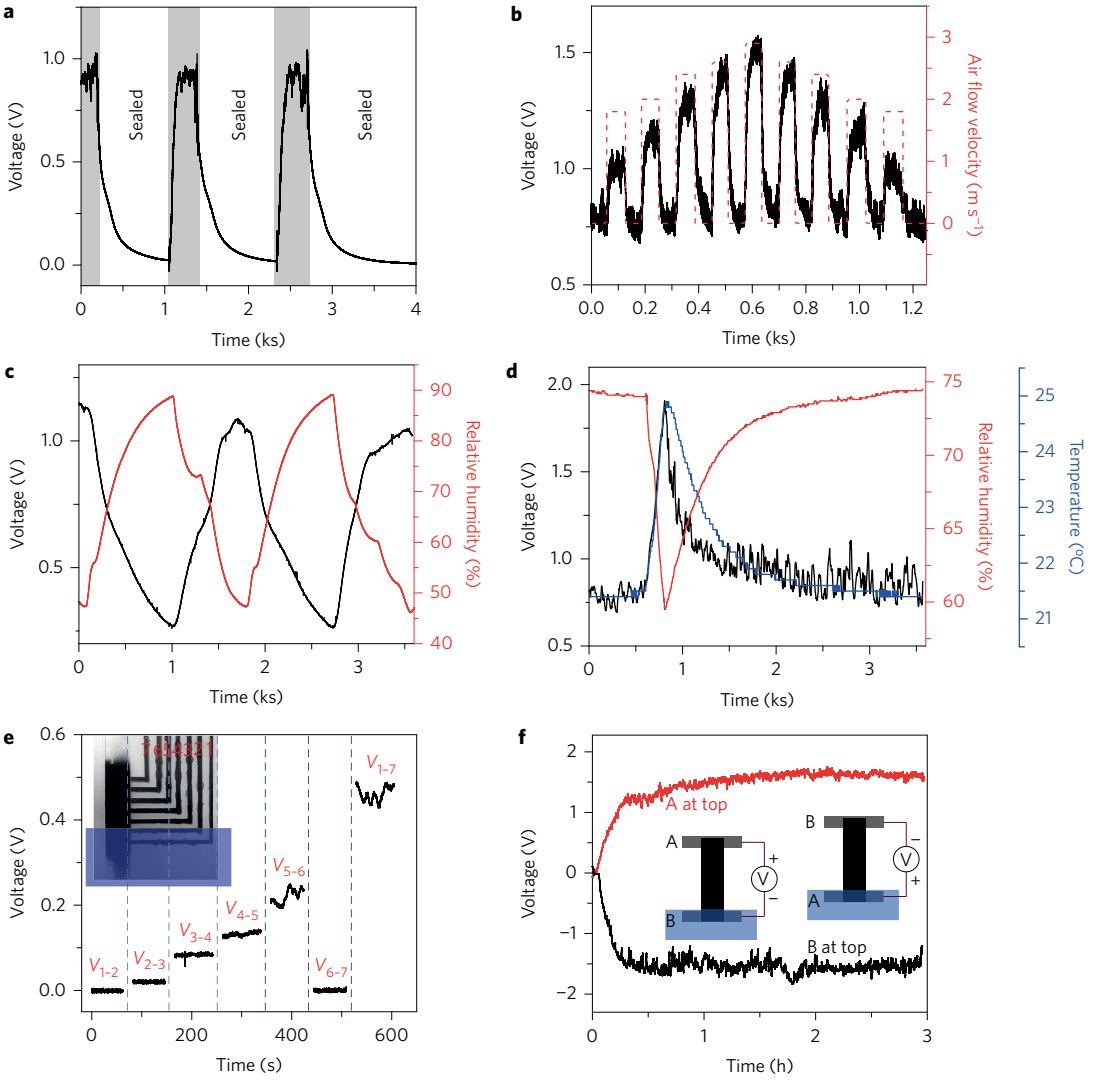

Figure 2 | Ambient conditions-dependent evaporation-induced potential. a, Measured V_{oc} of the device when the beaker was periodically sealed and unsealed. **b**, V_{oc} (black) enhanced by wind flow (red) with velocity of 1.9, 2.2, 2.4, 2.6 and 2.9 m s^{-1} in the laboratory environment. **c**, V_{oc} (black) variation as a function of relative ambient humidity (red) at a stable environmental temperature of ~22 °C. **d**, V_{oc} (black) variation as a function of environmental temperature (blue) and shift in ambient humidity (red). **e**, Saturated voltage differences between each two neighbouring electrodes of the seven-electrode device (inset) with the bottom two electrodes being inserted in water. The space of the electrodes is fixed at 5 mm. The ambient temperature in **a**,**b** and **e** is ~22 °C, and ambient relative humidity is ~70% in **a** and **b** and ~73% in **e**. **f**, Switching-polarity test of an evaporating-induced potential device. The induced voltage reverses its sign when the device is turned over without changing the electric circuit connection. Red and black curves are the corresponding V_{oc} of the device before and after it is turned over, respectively.

the sealed beaker is saturated at 100%, no evaporation occurs inside the beaker and the measured voltage should be attributed to water flow in the porous CB sheet driven by evaporation in the wet CB section outside the beaker.

Possible ions such as H^+ and OH^- are inevitable in the above experiments, although at very low concentration in the test system. We performed the evaporation-induced potential experiment similar to that in Fig. 1d with water containing different concentrations of NaCl. It is shown that the voltage decreases as the NaCl concentration increases from 10^{-7} mol l^{-1} to 1 mol l^{-1} nearly monotonically (Supplementary Fig. 15a). This ion concentration dependence is similar to that of the streaming potential induced by pressure-driven flow in nanochannels[19]. The zeta potential of the treated carbon film was measured to be about −33.2 mV (Supplementary Fig. 15b). Even without ions, our density functional theory (DFT) simulations have shown that electron redistribution at the interface of pure water and the functional graphene flakes can be significant enough for possible electrokinetic effects. As the evaporation-induced voltage and current can be stably sustained for several days (Fig. 1d and Supplementary Fig. 16) and rapidly drop once the sample is sealed in a beaker, and because the voltage response is negligible as the device is immersed in the water (Supplementary Fig. 11), a possible chemical reaction at the interface of carbon black should contribute little to the induced voltage. Other mechanisms such as electron drag[20], coupling of water[21] or molecular dipoles[22] and free charge carriers[23] may also have effects on the electricity generation in our system, which need intensive investigation in the future.

The evaporation-induced electricity has also been found in other kinds of carbon material, including MWCNT films, acetylene CB, toluene CB, pentanol CB and candle soot, although the induced potential varies largely with materials (Supplementary Fig. 17). The lowest evaporation-induced potential is measured in the nanotube sample on the order of 10 μV, whereas the highest

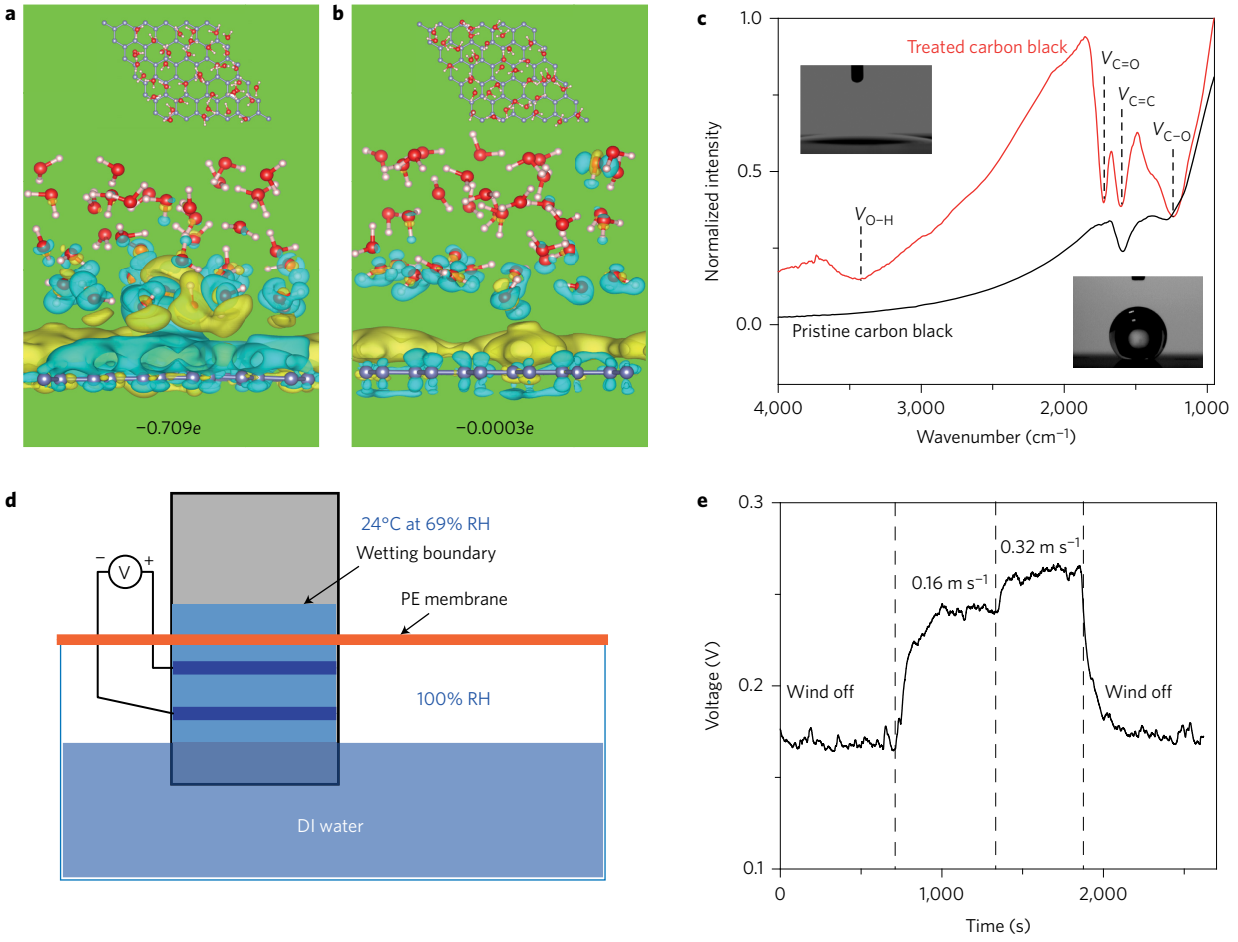

Figure 3 | Origin of the evaporation-induced electricity. a,**b**, Charge redistribution in functional C–O–C graphene (**a**) and pristine graphene (**b**) covered by three layers of water (yellow, gaining electron; blue, losing electron). The isosurface is set to 0.00015e Å^{-3}. Water-contact-induced electron redistribution in the carbon layer is labelled at the bottom of each panel. **c**, FTIR spectra of the pristine (black) and the annealing and plasma-treated (red) CB. Insets are water contact angle images of pristine CB (bottom right) and the annealing and plasma-treated CB (top left). **d**, Experiment set-up for evaporation-induced flow effect within the porous CB sheet. The bottom-half of the CB sheet with two electrodes at a spacing of 5 mm is sealed in the beaker by a PE membrane, while the top-half of the CB sheet is exposed to ambient air. **e**, Evaporation in the top-half induced a voltage between the two electrodes at different wind velocities.

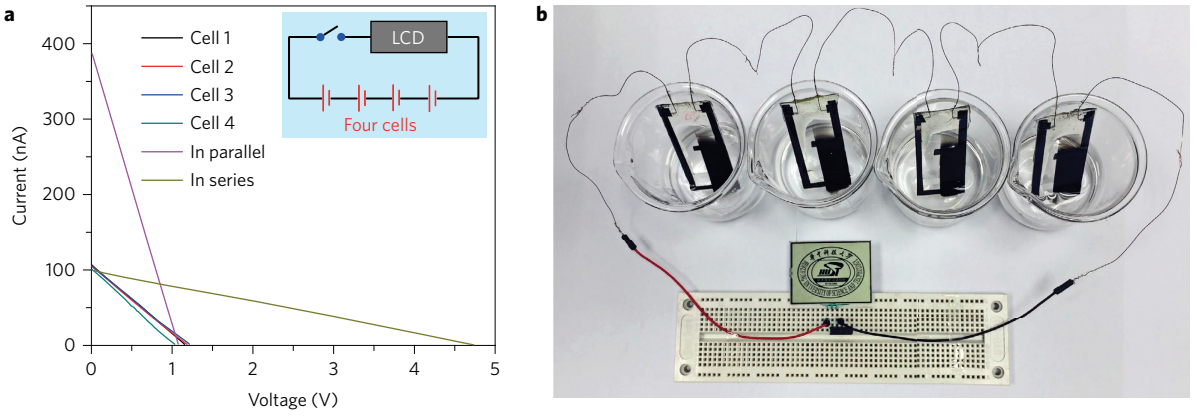

Figure 4 | Scaling and applications of the evaporation-induced electricity. a, Current–voltage curves of four individual devices and their series and parallel connections. Inset: circuit diagram. **b**, Photograph of an LCD driven by four devices connected in series. Each of the devices was fabricated in the same way as shown in Fig. 1a.

evaporation-induced potential around 1.3 V is obtained in toluene CB, which is comparable to that in the ethanol CB discussed above. The induced voltage in some ethanol CB samples can be up to 2 V (Supplementary Fig. 17a).

As has been shown in Fig. 1d, a centimetre-sized CB sheet can produce sustainable evaporation-induced potential around 1 V in ambient environment with peak output power up to 53 nW (Supplementary Fig. 18). It is practically important that the

output of the devices can be further scaled up simply through series and parallel connections of multiple devices as shown in Fig. 4a. When four small devices (with size of ~1.25 × 2.5 cm^2, V_{oc} of 1.1–1.25 V and I_{sc} of 100–105 nA; Supplementary Table 1) are connected in series, the evaporation-induced potential V_{oc} can be scaled up to 4.8 V, which is high enough to power a liquid crystal display (LCD) with a complicated picture as shown in Fig. 4b (Supplementary Movie 2). When the four devices are connected in parallel, the evaporation-induced I_{sc} can reach ~380 nA.

We have shown that water evaporation from a centimetre-sized CB sheet, with a thickness of a few micrometres, can generate a sustained voltage comparable to a standard AA battery. In comparison with the previously reported methods to harvest energy from complicated environments[24–26], such as vibration[27], solar, wind, and ocean energy[28], the electricity generation occurs in ambient environment, converting ambient thermal energy directly into electricity. In comparison with the classical streaming potential produced by an externally applied pressure gradient and other newly reported potentials created by, for example, gradients of temperature or chemical concentration, the electricity generation here is obtained through a natural process without mechanical work or artificial energy input. The evaporation-induced potential takes electric energy out of evaporation, which turns the sensible energy into latent heat. Furthermore, as water evaporation from carbon materials can be notably enhanced[29] and flow-induced potential can be optimized, it should be possible to design devices with enhanced electricity generation that can be used to complete essential tasks, such as sterilization, water purification and desalination. This approach could be of particular value in large-scale applications in warm regions on Earth.

Methods

Methods and any associated references are available in the online version of the paper.

Received 30 March 2015; accepted 20 December 2016; published online 30 January 2017

References

1. Penman, H. L. Natural evaporation from open water, bare soil and grass. *Proc. R. Soc. Lond. A* **193,** 120–145 (1948).
2. Bachhuber, C. Energy from evaporation of water. *Am. J. Phys.* **51,** 259–264 (1983).
3. Duan, F., Badam, V. K., Durst, F. & Ward, C. A. Thermocapillary transport of energy during water evaporation. *Phys. Rev. E* **72,** 056303 (2005).
4. Xu, J. *et al.* Large-scale synthesis of long crystalline $Cu_{2-x}Se$ nanowire bundles by water-evaporation-induced self-assembly and their application in gas sensing. *Adv. Funct. Mater.* **19,** 1759–1766 (2009).
5. Chen, X., Mahadevan, L., Driks, A. & Sahin, O. *Bacillus* spores as building blocks for stimuli-responsive materials and nanogenerators. *Nat. Nanotech.* **9,** 137–141 (2014).
6. Chen, X. *et al.* Scaling up nanoscale water-driven energy conversion into evaporation-driven engines and generators. *Nat. Commun.* **6,** 7346 (2015).
7. Wagenen, R. A. & Andrade, J. D. Flat plate streaming potential investigations: hydrodynamics and electrokinetic equivalency. *J. Colloid Interf. Sci.* **76,** 305–314 (1980).
8. Yin, J. *et al.* Waving potential in graphene. *Nat. Commun.* **5,** 3582 (2014).
9. Yin, J. *et al.* Generating electricity by moving a droplet of ionic liquid along graphene. *Nat. Nanotech.* **9,** 378–383 (2014).
10. Yuan, L. Y. *et al.* Carbon nanoparticles on carbon fabric for flexible and high performance field emitters. *Adv. Funct. Mater.* **21,** 2150–2154 (2011).
11. Jawhari, T., Roid, A. & Casado, J. Raman spectroscopic characterization of some commercially available carbon black materials. *Carbon* **33,** 1561–1565 (1995).
12. Portet, C., Yushin, G. & Gogotsi, Y. Electrochemical performance of carbon onions, nanodiamonds, carbon black and multiwalled nanotubes in electrical double layer capacitors. *Carbon* **45,** 2511–2518 (2007).
13. Deegan, R. D. *et al.* Capillary flow as the cause of ring stains from dried liquid drops. *Nature* **389,** 827–829 (1997).
14. Birdi, K. S., Vu, D. T. & Winter, A. A study of the evaporation rates of small water drops placed on a solid surface. *J. Phys. Chem.* **93,** 3702–3703 (1989).
15. Kresse, G. & Hafner, J. *Ab initio* molecular dynamics for liquid metals. *Phys. Rev. B* **47,** 558–561 (1993).
16. Kresse, G. & Furthmüller, J. Efficient iterative schemes for *ab initio* total-energy calculations using a plane-wave basis set. *Phys. Rev. B* **54,** 11169–11186 (1996).
17. Kresse, G. & Joubert, D. From ultrasoft pseudopotentials to the projector augmented-wave method. *Phys. Rev. B* **59,** 1758–1775 (1999).
18. Müller, J. O. *et al.* Morphology-controlled reactivity of carbonaceous materials towards oxidation. *Catal. Today* **102–103,** 259–265 (2005).
19. Van der Heyden, F. H. J., Bonthuis, D. J., Stein, D., Meyer, C. & Dekker & C. Power generation by pressure-driven transport of ions in nanofluidic channels. *Nano Lett.* **7,** 1022–1025 (2007).
20. Kárl, P. & Shapiro, M. Nanotube electron drags in flowing liquids. *Phys. Rev. Lett.* **86,** 131–134 (2001).
21. Zhao, Y. *et al.* Individual water-filled single-walled carbon nanotubes as hydroelectric power converters. *Adv. Mater.* **20,** 1772–1776 (2008).
22. Liu, Z. *et al.* Surface energy generator of single-walled carbon nanotubes and usage in a self-power system. *Adv. Mater.* **22,** 999–1003 (2010).
23. Yin, J., Zhang, Z. H., Li, X. M., Zhou, J. X. & Guo, W. L. Harvesting energy from water flow over graphene? *Nano Lett.* **12,** 1736–1741 (2012).
24. Yan, Y., Timoner, J. V. I. & Grzybowski, B. A. A long-lasting concentration cell based on a magnetic electrolyte. *Nat. Nanotech.* **9,** 901–906 (2014).
25. Dresselhaus, M. S. & Thomas, I. L. Alternative energy technologies. *Nature* **414,** 332–337 (2001).
26. Wu, W. Z. *et al.* Piezoelectricity of single-atomic-layer MoS_2 for energy conversion and piezotronics. *Nature* **514,** 470–474 (2014).
27. Saadon, S. & Sidek, O. A review of vibration-based MEMS piezoelectric energy harvesters. *Energy Convers. Manage.* **52,** 500–504 (2011).
28. Khaligh, A. & Onar, O. C. *Energy Harvesting: Solar, Wind, and Ocean Energy Conversion Systems* (CRC Press, 2010).
29. Ghasemi, H. *et al.* Solar steam generation by heat localization. *Nat. Commun.* **5,** 4449 (2014).

Acknowledgements

This work was financially supported by the National Natural Science Foundation of China (51322210, 51672097, 51472117, 51535005), 973 programs (2013CB932604), a Foundation for the Author of National Excellent Doctoral Dissertation of PR China (201035), the National Program for Support of Top-notch Young Professionals and Director Fund of WNLO. We thank Y. Gogotsi, M. Xu, J. Tang, S. Q. Zeng, K. Lu, H. J. Gao, X. C. Zeng, Z. L. Wang and Z. H. Zhang for helpful discussions and suggestions, and K. Liu for help in the streaming potential test.

Author contributions

J.Z. and W.G. conceived and designed the study; G.X., T.D., J.L., W.F., J.Yin, Y.C. and L.Y. performed the experiments, Y.X. and J.Yu conducted the simulations; L.G., J.C. and S.D. took part in characterizing the samples; W.G. and J.Z. analysed the results with contributions from all authors and wrote the manuscript.

Additional information

Supplementary information is available in the online version of the paper. Reprints and permissions information is available online at www.nature.com/reprints. Correspondence and requests for materials should be addressed to J.Z. and W.G.

Competing financial interests

The authors declare no competing financial interests.

Methods

Chemicals and reagents. Multiwalled carbon nanotubes (MWCNTs) were purchased from XF Nano. Sulfuric acid (H_2SO_4), nitric acid (HNO_3), ethanol, propanol, butanol, pentanol, hexane and candle were purchased from Sinopharm Chemical Regent. Acetylene CB was purchased from Alfa Aesar. Quartz plates ($25 \times 75 \times 1$ mm^3 for two-electrode devices and $50 \times 75 \times 1$ mm^3 for multiple-electrode devices) were purchased from Jinghe Optical Instruments corp.

Synthesis of soluble MWCNT ink. Typically, 3 g of MWCNTs was dispersed by sonication in 130 ml mixed H_2SO_4 and HNO_3 ($H_2SO_4/HNO_3 = 3/1$, v/v) solution for 10 min. Then, the MWCNT–acid mixture was refluxed while stirring vigorously for 2.5 h in a 90 °C oil bath. The mixture was allowed to cool at room temperature after the refluxing process. The MWCNTs extracted from the residual acids were purified by repeating the processes: diluting with distilled water, centrifuging and decanting the solutions. When the supernatant was neutral, the treated MWCNTs were redispersed in DI water with a concentration of 10 mg ml^{-1}, forming a MWCNT ink.

Fabrication of the CB devices. Quartz plates were cleaned ultrasonically in acetone, alcohol and pure water and were dried in a 70 °C oven. Then, MWCNT ink was printed on the quartz with desired patterns by a floating knife coater, which served as the electrode. The electrodes were about 1.5 μm thick and 2 mm wide, with resistance measured to be ~2 kΩ sq^{-1}. For a two-electrode device, the space between the two electrodes was 2.5 cm. Whereas for multiple-electrode devices, the space between the centre of two neighbouring electrodes was 5 mm. CB sheets were locally grown on the quartz plate using a quartz mask through an ethanol (or toluene, pentanol) flame synthesis method[10]. In a typical synthesis process, the quartz substrate was mounted in the flame core 5.5 cm above the wick for 5 min with surface temperature of 790–830 °C, while commercial acetylene CB (Alfa Aesar) was printed on the quartz plate with two MWCNT electrodes. After annealing in air at 370 °C for 150 min and cooling to room temperature, the CB sheet was treated with air plasma (pressure 100 Pa, RF power 130 W) for 60 s in a plasma cleaner (Mingcheng, PDC-MG). Subsequently, enameled wires were bonded to the ends of the MWCNT electrodes by conductive carbon tapes. Finally, all of the exposed MWCNT electrode regions were encapsulated by epoxy to avoid contacting with the liquid when the device is immersed.

Material characterizations. The morphology, structure and functional groups of CB were characterized by scanning electron microscope (FEI Nova Nano450), high-resolution transmission electron microscope (Titan G^2 60-300 probe Cs corrector), Quantachrome Autosorb-1C-VP instrument, Fourier-transform infrared spectrometer coupled with infrared microscope (Bruker Vertex 70), X-ray photoelectron spectrometer (ESCALab250) and Raman spectrometer (Renishaw-inVia, 514.5 nm line of an Ar$^+$ laser). The contact angle of water droplets on CB layer was measured by a Kino SL200B Contact Angle meter.

Device characterizations. After the device was completely wetted by DI water, the device was inserted into a beaker (100 ml beaker was used for two-electrode device test whereas 150 ml beaker was used for multi-electrode device test), then DI water was added to the beaker with a syringe until the water level reached the bottom electrode of the device. The current–voltage characterization of the device was measured by Keithley 2400. The open-circuit voltage (V_{oc}) of the device was measured by Keithley 2000 and the short-circuit current (I_{sc}) was measured by a low-noise current preamplifier (SRS Model SR570). The environmental temperature and humidity were recorded by Center 310 Rs-232 Humidity Temperature Meter.

To investigate the V_{oc} variation as a function of wind flow velocity, a fan with controllable speed was used and the flow velocity was monitored by an anemograph (Tecman TM826).

To investigate the V_{oc} variation as a function of relative ambient humidity, the device was placed in a testing space with controllable N_2 supply system (Supplementary Fig. 19). The gas flow was divided into two paths by a set of silicon tubes, one tube was connected to dry N_2 directly; the other tube was interrupted by a gas bottle that was filled with water and immersed in a thermo tank. In this case, certain water vapour would be brought out of the tube depending on the temperature of hot water when N_2 passed through the gas bottle. The humidity of the space could be adjusted by controlling the water vapour flow ratio and the water temperature. The total gas flow was fixed at 200 l h^{-1}. The relative humidity and temperature was monitored in real time by a Center 310 Rs-232 Humidity Temperature Meter.

To investigate the V_{oc} variation as a function of environmental temperature as well as the relative ambient humidity, an infrared bulb was used as a heating source to increase the environmental temperature from 21.4 to 25 °C, while the environment relative humidity dropped in accordance from 75 to 60%. The relative humidity and temperature was monitored in real time by a Center 310 Rs-232 Humidity Temperature Meter.

To investigate the thermoelectric effect on the device, one end of the device was fixed on a heater that was controlled by a Lakeshore 335 Temperature Controller, and the other end was fixed on a big stainless steel plate that acted as a cooler. The heater was heated from ~22 °C to 94.3 °C and then cooled to room temperature. Meanwhile, the induced voltage was monitored. To investigate the output of the device, different loads with resistance of 0.5, 1, 2, 4, 6, 8, 10, 20, 40, 60, 80 and 100 MΩ were connected with the device, respectively. The voltage drop (V) and current (I) across different load were recorded.

Computational method. First-principles calculations were performed within the framework of DFT as encoded in Vienna Ab-initio Simulation Package code[15–17]. The projector-augmented wave method for the core region and the Perdew–Burke–Ernzerhof (PBE) functional for the exchange-correlation potential were employed[30]. The van der Waals interactions were considered in the calculations. The kinetic energy cutoff of the plane-wave expansion was set to be 500 eV. The geometry was fully relaxed with the conjugate gradient method until the force on each atom was less than 0.01 eV Å^{-1}. The convergence for energy was chosen as 10^{-4} between two consecutive steps for geometric optimize and 10^{-5} for static calculations.

To elucidate the mechanism, three theoretical models based on DFT calculations were built in this work. For all cases, the vacuum between two adjacent planes was set larger than 20 Å to avoid the interactions between period images. And charge redistribution was defined as $\Delta\rho = \rho_{FG+w} - \rho_{FG} - \rho_w$, where ρ_{FG+w}, ρ_{FG} and ρ_w denote the charge distribution of the whole adsorption system, graphene with functional groups and water molecule. To give a direct comparison of numerical values for electron transfer, Bader analysis was used to calculate the charge transfer in atoms.

To study the water adsorption on the surface of (functional) graphene, water molecules adsorbed on a 6×6 supercell of graphene were compared without/with functional groups. The Brillouin zone was sampled with $2 \times 2 \times 1$ grid for geometric optimize and $6 \times 6 \times 1$ grid for static calculations. Typically, for -O functional group, the oxygen atom was adsorbed between the two nearest carbon atoms, forming the C–O–C triangle structure. The calculation results of when the C–O–C graphene and pristine graphene are covered by three layers of water are presented in Fig. 3a,b.

Data availability. All data generated or analysed during this study are included in this published article (and its Supplementary Information files).

References

30. Perdew, J. P., Burke, K. & Ernzerhof, M. Generalized gradient approximation made simple. *Phys. Rev. Lett.* **77,** 3865–3868 (1996).